



Since January 2020 Elsevier has created a COVID-19 resource centre with free information in English and Mandarin on the novel coronavirus COVID-19. The COVID-19 resource centre is hosted on Elsevier Connect, the company's public news and information website.

Elsevier hereby grants permission to make all its COVID-19-related research that is available on the COVID-19 resource centre - including this research content - immediately available in PubMed Central and other publicly funded repositories, such as the WHO COVID database with rights for unrestricted research re-use and analyses in any form or by any means with acknowledgement of the original source. These permissions are granted for free by Elsevier for as long as the COVID-19 resource centre remains active.



Sensitive fluorescence biosensor for SARS-CoV-2 nucleocapsid protein detection in cold-chain food products based on DNA circuit and g-CNQDs@Zn-MOF

Chen Zhou^a, Chiliang Lin^a, Yuyao Hu^a, Haocheng Zan^a, Xiaruiyan Xu^a, Chengjun Sun^{a,c}, Haimin Zou^{b,*}, Yongxin Li^{a,c,**}

^a West China School of Public Health and West China Fourth Hospital, Sichuan University, Chengdu, 610041, China

^b Department of Clinical Laboratory, Sichuan Cancer Hospital and Institute, Sichuan Cancer Center, School of Medicine, University of Electronic Science and Technology of China, Chengdu, 610041, China

^c Provincial Key Laboratory for Food Safety Monitoring and Risk Assessment of Sichuan, Chengdu, 610041, China

ARTICLE INFO

Keywords:

SARS-CoV-2
Conformational entropy-driven circuit
Aptamer
G-CNQDs@Zn-MOF
Cold-chain food product

ABSTRACT

SARS-CoV-2 isolation from cold-chain food products confirms the possibility of outbreaks through cold-chain food products. RNA extraction combined with RT-PCR is the primary method currently utilized for the detection of SARS-CoV-2. However, the requirement of hours of analytical time and the high price of RT-PCR hinder its worldwide implementation in food supervision. Here, we report a fluorescence biosensor for detection of SARS-CoV-2 N protein. The fluorescence biosensor was fabricated by aptamer-based conformational entropy-driven circuit where molecular beacon strands were labeled with graphitic carbon nitrides quantum dots@Zn-metal-organic framework (g-CNQDs@Zn-MOF) and Dabcyl. The detection of the N protein was achieved via swabbing followed by competitive assay using a fixed amount of N-48 aptamers in the analytical system. A fluorescence emission spectrum was employed for the detection. The detection limit of our fluorescence biosensor was 1.0 pg/mL for SARS-CoV-2 N protein, indicating very excellent sensitivity. The fluorescence biosensor did not exhibit significant cross-reactivity with other N proteins. Finally, the biosensor was successfully applied for the detection of SARS-CoV-2 N protein in actual cold-chain food products showing same excellent accuracy as RT-PCR method. Thus, our fluorescence biosensor is a promising analytical tool for rapid and sensitive detection of SARS-CoV-2 N protein.

1. Introduction

In September 2020, epidemiological information on clusters of Corona Virus Disease 2019 (COVID-19) cases in Qingdao, China and genomic sequencing confirmed that two dock workers were infected after contact with the contaminated outer packaging. Moreover, the sequences from the dock workers and the package materials differed by 12–14 nucleotides of Wuhan reference strain. In addition, infectious virus in the cold-chain products was isolated by cell culture, and typical severe acute respiratory syndrome coronavirus 2 (SARS-CoV-2) particles were observed with electron microscopy (Huילai et al., 2021). Food contamination of SARS-CoV-2 has attracted considerable attention in many areas and countries, since it posed a risk for virus spreading

(Ceylan, Meral, & Cetinkaya, 2020; Chi, Wang, Chen, & Zheng, 2021; Liu et al., 2020). As a matter of fact, there were frequent reporters on positive identification of SARS-CoV-2 in cold-chain food products around the world recently, including the SARS-CoV-2 confirmed on plastic packing. Due to the temperature below 0 °C during the cold-chain transportation, the SARS-CoV-2 could survive longer than in room temperature environment (Godoy, Kibenge, & Kibenge, 2021; Haddow et al., 2020; Yekta, Vahid-Dastjerdi, Norouzbeigi, & Mortazavian, 2021). Besides, the concentration of virus in food may be of trace level. Therefore, sensitive, rapid, low-cost and rapid detection of SARS-CoV-2 is urgently needed for effective control of the transmission via cold-chain food products.

SARS-CoV-2 has four main structural antigens, including

* Corresponding author.

** Corresponding author. West China School of Public Health and West China Fourth Hospital, Sichuan University, Chengdu, 610041, China.

E-mail addresses: zhm504532@163.com (H. Zou), liyongxin@scu.edu.cn (Y. Li).

<https://doi.org/10.1016/j.lwt.2022.114032>

Received 2 March 2022; Received in revised form 21 September 2022; Accepted 24 September 2022

Available online 26 September 2022

0023-6438/© 2022 The Authors. Published by Elsevier Ltd. This is an open access article under the CC BY-NC-ND license (<http://creativecommons.org/licenses/by-nc-nd/4.0/>).

nucleocapsid (N), spike (S), matrix (M), and envelope (E) (Wang et al., 2020). Among them, the N and S proteins have the potential to be utilized as biomarkers owing to their distinguishability to different types of corona viruses (Kirtipal, Bharadwaj, & Kang, 2020). SARS-CoV-2 was initially diagnosed using reverse transcription polymerase chain reaction (RT-PCR). RT-PCR takes at least 3 h, including preparation of viral RNA which is key to guaranteeing diagnostic accuracy (Ozma et al., 2020; Rahimi, Mirzazadeh, & Tavakolpour, 2021). Considering the increasing number of food samples that may be contaminated, the RT-PCR kit has not been able to meet the testing demand. Moreover, the wide applicability of RT-PCR for large scale analysis of SARS-CoV-2 is hindered, owing to relatively high cost, especially in middle- and low-income countries. Hence, highly sensitive immunological analytical assays which could directly detect viral antigens in cold-chain food products are necessary for timely detection of SARS-CoV-2 and cutting off transmission routes.

Biosensors have been widely employed in analytical applications, suggesting easy, rapid, and reliable detection (Ragavan, Kumar, Swaraj, & Neethirajan, 2018; Vermisoglou et al., 2020; Yang et al., 2019). Previously, various kinds of biosensors were reported for the detection of viruses, including surface plasmon resonance (Bocková, Slabý, Špringer, & Homola, 2019; Zhao, Tong, Xia, & Peng, 2019), electrochemical (De la Paz et al., 2021; Leung, Downs, Ortega, Kurnik, & Plaxco, 2021; Sun, Sun, Yang, Jin, & Gui, 2021), fluorescent (Selby, Aurelio, Yuen, Graham, & Johnston, 2018; Wang, Gong, et al., 2020), and colorimetric (Fu et al., 2021; Lopreside et al., 2021; Pan et al., 2021) assays. Among these methods, fluorescent analysis is popular due to its simple operation, high sensitivity and good selectivity, which hold the potential to be used by the public with acceptable sensitivity. As the next generation of light-emitting materials, semiconductor quantum dots (QDs) have many unique properties such as narrow band-edge photoluminescence and broad absorption range with high emission quantum yield, and have been attracting considerable attention (Owen & Brus, 2017; Reiss, Protière, & Li, 2009). Among them, graphitic carbon nitrides quantum dots (g-CNQDs) are the carbon material rich in nitrogen with the graphitized structure (Vashisht et al., 2020). The applied research on g-CNQDs have been a research hotspot owing to good optical properties, water solubility, low toxicity and good biocompatibility (Kong et al., 2020; Shao et al., 2019). An important technology for the fabrication of such QD-based fluorescence biosensors is the development of matrices to exist between the particles, which need to ensure the stable fluorescence performance and adequately optical characteristics of each QD. Attempts to embedding QDs into solid materials have been made to prevent QDs against the possible damage generated by oxygen species (Loiudice, Saris, Oveisi, Alexander, & Buonsanti, 2017; Sun et al., 2017). In 2019, Kumagai, Uematsu, Torimoto, and Kuwabata (2019) employed metal-organic frameworks (MOF) as a surface modifier to maintain the long-term stability of QDs, which indicated the application prospects of QD@MOF in fluorescence sensors.

Aiming to detecting proteins, the structural switching of DNA aptamers and other DNA-based structures containing recognition elements have been widely utilized to develop the fluorescence sensors (Chen, Wu, Chen, Ni, & Dai, 2020; Liu et al., 2018; Yousefi, Ali, Su, Filipe, & Didar, 2018). DNA self-assembly techniques, including hybridization chain reaction (HCR), and catalytic hairpin assembly (CHA), are often utilized as signal amplification strategies in the aptamer-based biosensors (Zhou et al., 2018). However, the signal leakage of these DNA self-assembly reactions, based on hairpin structure, resulted in high background signals. It's reported that the reaction, driven by the configurational entropy of the released molecule, could effectively reduce the background signal (Zhang, Turberfield, Yurke, & Winfree, 2007). Configurational entropy-driven circuit allows restricted input oligonucleotides to facilitate the release of specific output oligonucleotides, which in turn can act as catalysts for other reactions. Fan et al. (2021) developed a DT-based electrochemiluminescence biosensor for the sensitive assay of RdRp gene via entropy-driven cascade amplifying

strategy. Given the modularity and scalability of entropy-driven DNA circuit, the versatility of diverse DNA target was prone to implementation without any involvement of nuclease, demonstrating the excellent advantages in cost, sensitivity, operation.

Here, we proposed a combination configurational entropy-driven DNA circuit and fluorescent assay for the detection of SARS-CoV-2 N protein. In this work, the aptamer-based configurational entropy-driven DNA circuit plays a dual-functional role as exclusive target recognition and signal enhancement in biosensor. Molecular beacon (MB) strands, modified with g-CNQDs@Zn-MOF and quenching group (Dabcyl), were utilized as signal converters which could provide specific and stable fluorescent signal quickly. Subsequently, the fluorescence biosensor was applied in the determination of cold-chain food products. In the future, as a variety of aptamers will be available or can be developed through systematic evolution of ligands by exponential enrichment (SELEX), the conformational entropy-driven DNA circuits developed in this study can be applied to the analyses of targets other than the SARS-CoV-2 N protein.

2. Experimental methods

2.1. Pretreatment of DNA strands

Based on the sequence of the aptamer of SARS-CoV-2 N protein (N-48) (Zhang et al., 2020), catalyst strand (C), fuel strand (F), three-stranded substrate complex (S) consisting of S1 strand, output strand (OP), signal (SB) strand, and MB strand, were designed using NUPACK software (<http://www.nupack.org>). DNA strands were synthesized and purified by Sangon Biotech Co., Ltd (Sangon Biotech, China). The DNA sequences were shown in Table 1.

2.2. Preparation and characterization of g-CNQDs@Zn-MOF

The compounds of 0.081 g (0.28 mmol) sodium citrate and 0.101 g (1.68 mmol) urea were ground into uniform powder in a mortar. The mixed system was added into the autoclave, and baked at 180 °C for 1 h. After being naturally cooled to room temperature, the yellow product was washed 3 times with ethanol. To obtain g-CNQDs, the yellow product was dialyzed in pure water using a dialysis membrane (retained molecular weight 500 Da) for 24 h.

The reaction solutions were prepared as following: 0.58 g (2.0 mmol) zinc nitrate hexahydrate (Kar-Fischer Reagent, China), 0.35 g (2.0 mmol) *p*-Phthalic acid (H₂BDC, Huaxia Chemical Reagent, China), and 0.11 g (1.0 mmol) diethylenediamine (TED, Huaxia Chemical Reagent, China) were dissolved in 20, 10, and 20 mL dimethylformamide (DMF, Kar-Fischer Reagent, China), respectively. H₂BDC and TED were slowly added into zinc nitrate solution, and the mixed substances reacted in an autoclave at 120 °C for 24 h. After being naturally cooled to room temperature, the product was separated by filtration. Subsequently, the resulting product was washed 3 times with DMF, and the DMF was removed at 80 °C in N₂ atmosphere to obtain Zn-MOF.

To obtained uniformly dispersed aqueous solution of Zn-MOF, 5 mg Zn-MOF was dissolved in 20 mL ddH₂O, and ultrasonicated at 20 °C for 1 h. Then, 300 μL g-CNQDs was added into aqueous solution of Zn-MOF, g-CNQDs@Zn-MOF was obtained after sonication for 2 h.

Morphology and particle size of g-CNQDs, Zn-MOF and g-CNQDs@Zn-MOF were characterized with scanning electron microscope (SEM), also, the fluorescence emission spectra of the above nanomaterials were measured.

2.3. Biofunctionalization of g-CNQDs@Zn-MOF

Prior to modification on the surface of g-CNQDs@Zn-MOF, MB strands were incubated with 0.35% glutaraldehyde for 4 h at room temperature. Then, the final mixed system of MB strands and g-CNQDs@Zn-MOF was centrifuged at 12000 rpm/min for 30 min (Fresco

Table 1
Sequences of DNA fragments.

Name	Sequence(5'→3')
N-48 aptamer	GCTGGATGTCGCTACGACAATATTCCTTAGGGGCACCGCTACATTGACACATCCAGC
S1	CCTACGTCTCCAACCTAAGTACGGCCCTTCATTGACACATCCAGCTCTCC
OP	CCGTAAGTTAGTTGGAGACGTAGGCTTCCTACA
SB	GCTGGATGTCGAATGAAGGGCCACATACATCATATT
C	GGAGAGCTGGATGTGTCATG
F	GCTGGATGTCGAATGAAGGGCCGTAAGTTAGTTGGAGACGTAGG
MB	NH ₂ C ₆ -GGCCAATATGATGTATGTGGCCCTTGCC-Dabcy1

17, Thermo, the U.S.), and the precipitation was washed 3 times with DPBS (137 mmol/L NaCl, 2.7 mmol/L KCl, 1.5 mmol/L KH₂PO₄, 8 mmol/L Na₂HPO₄, 1 mmol/L CaCl₂, 0.5 mmol/L MgCl₂, pH 7.4) to remove free MB strands. Finally, the biologically functional g-CNQDs@Zn-MOF with MB strands was resuspended in DPBS and stored at 4 °C.

2.4. Detection of N protein with fluorescence biosensor

A series of concentrations (5.0 pg/mL~1.0 × 10³ pg/mL) of N proteins (Sangon Biotech, Shanghai, China) reacted with 200 nmol/L N-48 aptamers, 200 nmol/L S strands, 200 nmol/L C strands, 300 nmol/L F strands, and 200 nmol/L g-CNQDs@Zn-MOF-tagged MB strands in a final volume of 500 μL DPBS system at room temperature for 30 min, respectively. All fluorescence emission spectra were observed using fluorescence spectrophotometer (HITACHI, F-4700, Japan), and the measurement conditions were as follows: excitation light wavelength was 375 nm with slit width of 5 nm, and the emission spectra were recorded in the range of 400–600 nm with slit width of 5 nm; the scanning speed was 1200 nm/min, and the PMT was 700 V. Quantitative analysis of N proteins was obtained based on photoluminescence (PL) intensity.

2.5. Determination of actual samples

64 cold-chain food products (including cherry, frozen shrimp, salmon, and frozen fish), imported from Brazil, Uruguay and Argentina, were sampled with swab method: the whole animal foods were sampled by smearing the surface of the animal, mouth and other detectable cavity spaces; the segmented animal products were just sampled by smearing the surface. Plant foods were sampled by smearing the surface, including surface crevices. The disposable long-handled sampling swab impregnated with sterile PBS, was utilized to smear 5 times on each surface horizontally and vertically, with rotating the sampling swab. After the part touched by the hand was cut off, the swab was placed in a sampling tube containing 3.0 mL PBS, and the sampling was completed by making a record.

After heating at 95 °C for 10 min, sample solution of 200 μL was analyzed with the biosensing strategy established in this study. N proteins were detected in the cold-chain food products, and the test results using this fluorescence biosensor, were compared with the results of RT-PCR (2019-nCoV Nucleic Acid Detection Kit, Sansure Biotech, China). The RT-PCR was carried out according to following manufacturer's instructions.

2.6. Statistical analysis

SARS-CoV-2, detected with the fluorescence aptasensor was deemed positive when PL intensity exceeded the threshold level (the PL intensity of LOD). Following manufacturer's instructions, the SARS-CoV-2, detected with the RT-PCR method was deemed negative when Ct-value exceeded 38. The sensitivity, specificity, positive predictive value, and negative predictive value were analyzed with SPSS 21.0 software (IBM, Chicago, IL).

3. Results and discussion

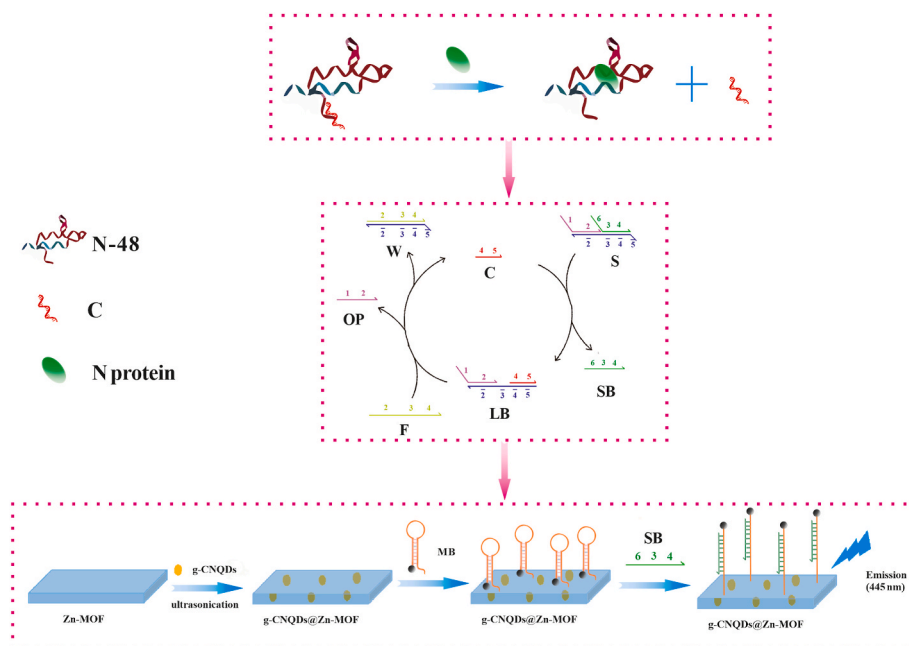
3.1. The principle of the fluorescence biosensor

We established a robust fluorescence biosensor based on nonenzymatic DNA circuit and demonstrated the potential of conformational entropy-driven DNA circuit as powerful signal amplification. The introduction of N-48 aptamer provided a direct molecular bridge between N protein and DNA, enabling sensitive and highly specific sensing of SARS-CoV-2. The main achievement was that DNA circuits could be readily matched and mixed due to the supernormal programmability provided by conformational entropy and interactions of base-pairing. Besides, the stability and reproducibility of this fluorescence biosensor are significantly enhanced.

In the reaction driven by conformational entropy, catalyst strand (C) and fuel strand (F) reacts with the three-stranded substrate complex (S), displacing output (OP) and signal strands (SB) from linker strand (LB) to form waste complex (W). The total number of base pairs in the reactants and products is unchanged, and the reaction was driven forward thermodynamically by the entropic gain of the liberated molecules. Hence, with the assistance of toehold, two continuous strand displacement assembly (SDA) reactions can be carried out in the predetermined direction, and a more complex reaction network would be constructed. The sensing strategy established in this study was illustrated in Scheme 1. When N protein was absent from the system, fluorescent signal of g-CNQDs@Zn-MOF was quenched by quenched groups (Dabcy1), resulting in weak background fluorescent signal. When the N protein was present in the system, the N-48 aptamer would specifically bind with the N protein, and strand C was released to the reaction system. Free strand C could hybridize with complex S via the toehold region $\bar{5}$, so that the strand SB was replaced, leading to the exposure of a new toehold region $\bar{3}$. Subsequently, the F could replace the strand C and strand OP via toehold region $\bar{3}$ mediated SDA. Free strand C would trigger new circuits, thereby a large number of strand SB were released. Consequently, strand SB could bind with MB strand conjugated on g-CNQDs@Zn-MOF, and the fluorescent signal was restored since the fluorescent group and the quenching group in MB strand were separated. Therefore, quantitative analysis of the N protein could be realized, according to the intensity of the fluorescent signal. Compared with the previous SDA based on the hairpin substrates, the signal leakage of the linear DNA-based SDA driven by conformational entropy is much lower, and this conformational entropy-driven DNA circuit could amplify signals significantly while keeping lower background by rational sequence design.

3.2. Characterization of g-CNQDs, Zn-MOF and g-CNQDs@Zn-MOF

The SEM images of g-CNQDs, MOF and g-CNQDs@Zn-MOF were exhibited in Fig. 1. The diameter of g-CNQDs prepared in this study was about 72–90 nm with a well-shaped spherical structure (Fig. 1A). Zn-MOF has a three-dimensional frame structure (Fig. 1B). Fig. 1C and D showed SEM images of g-CNQDs@Zn-MOF with different magnifications. Compared with Zn-MOF, there is no obvious change in the three-dimensional frame structure of g-CNQDs@Zn-MOF. As SEM results suggested that g-CNQDs were successfully encapsulated in Zn-MOF



Scheme 1. Detection of N protein with the proposed fluorescent biosensor based on DNA circuit and g-CNQDs@Zn-MOF. Abbreviation: aptamer of N protein (N-48), catalyst strand (C), fuel strand (F), three-stranded substrate complex (S), displacing output (OP), signal strands (SB), linker strand (LB), waste complex (W) and molecular beacon (MB).

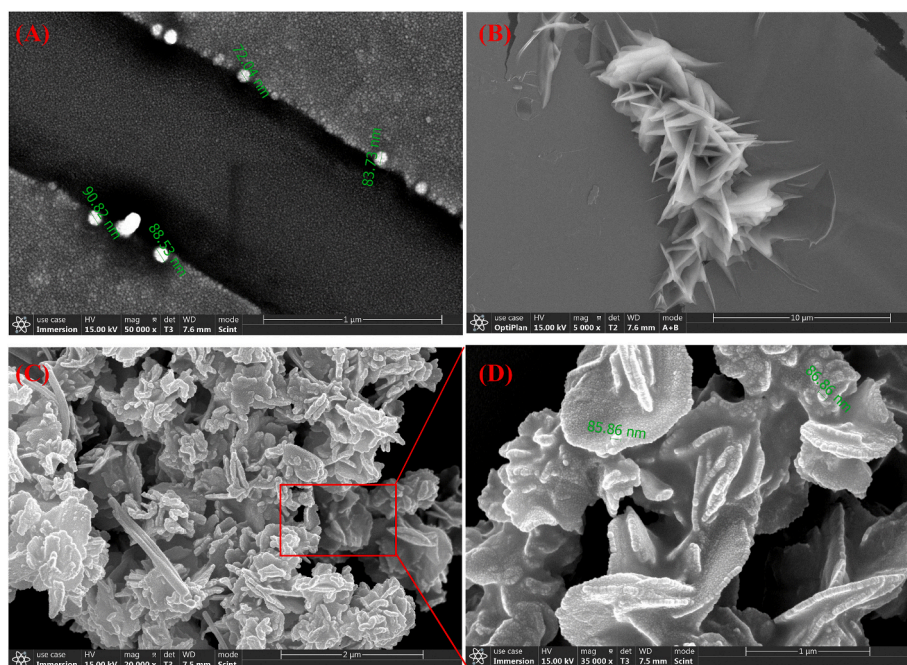


Fig. 1. Scan electron micrographs of (A) g-CNQDs, (B) Zn-MOF, (C&D) g-CNQDs@Zn-MOF.

without affecting the main structure of Zn-MOF.

3.3. Fluorescence properties of g-CNQDs, Zn-MOF and g-CNQDs@Zn-MOF

The fluorescence emission spectra of g-CNQDs, Zn-MOF and g-CNQDs@Zn-MOF were exhibited in Fig. 2. The maximum emission wavelengths of Zn-MOF and g-CNQDs@Zn-MOF were 425 nm and 440 nm, respectively. The fluorescence intensity of Zn-MOF was the weakest, and the fluorescence signals of g-CNQDs@Zn-MOF was slightly higher

than g-CNQDs, indicating that MOF had a positive effect on photoelectric properties of g-CNQDs. In addition, g-CNQDs and g-CNQDs@Zn-MOF were exposed in the air for a long time, and their fluorescence intensity were continuously monitored. It was found that the fluorescence signal of g-CNQDs attenuated significantly after 24 h, while the fluorescent signal g-CNQDs@Zn-MOF didn't show a remarkable decrease even after 2 weeks (Fig. S3). The reason might be that MOFs with regular structure could enhance the photoelectric properties of g-CNQDs and provide additional stability for better sensing performance.

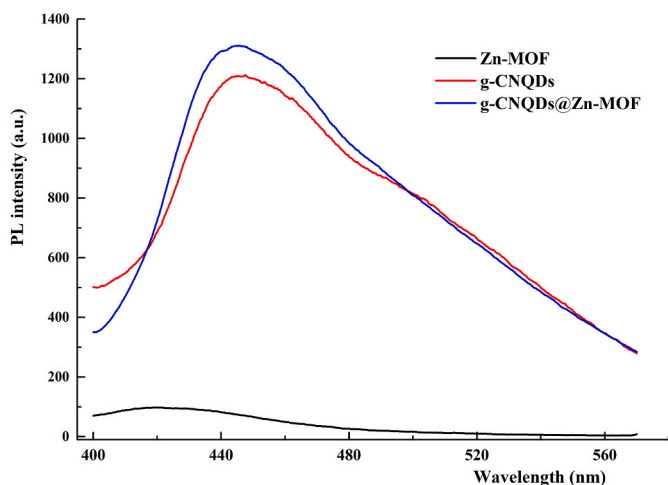


Fig. 2. Fluorescence emission spectra of g-CNQDs, Zn-MOF and g-CNQDs@Zn-MOF.

3.4. Optimization of toehold length and F strand concentration

In the enzyme-free DNA circuit driven by conformational entropy, the length of the exposed toehold region $\bar{5}$ and the hidden toehold region $\bar{3}$ were able to affect the initiation of the SDA; furthermore, the concentration of strand F has a significant influence on specificity and efficiency of the conformational entropy-driven circuit. The efficiency and specificity of the SDA were investigated when the base number of toehold region $\bar{5}$ and toehold region $\bar{3}$ were 6 nt/4 nt, 5 nt/5 nt, and 4 nt/6 nt, respectively, with the different ratios of the concentration of strand F to complex S (the concentration of complex S remained at 200 nmol/L). As demonstrated in Fig. 3, when the number of bases in the toehold region $\bar{5}$ was 4 nt, the reaction efficiency between strand S and strand C was the lowest. As the number of bases in the toehold region $\bar{5}$ increased, the bands of complex LB became more and more visible and the reaction efficiency between strand C and strand S gradually increased. Besides, when the number of bases in toehold region $\bar{3}$ was 4 nt, the reaction efficiency of between strand F and complex LB was the lowest. As the number of bases increased in toehold region $\bar{3}$, the amount of complex W was significantly improved. Taking into account of the binding efficiency of strand C and complex S, and the replacement efficiency of strand OP by the strand F, the number of bases in the toehold region $\bar{5}$ and region $\bar{3}$ are designed both 5 nt. Next, the reaction efficiency of each conformational entropy-driven circuit system with different concentration ratios of strand F to strand S (0.5:1, 1:1, 1.5:1, 2:1) was investigated. The results showed that as the ratio of strand F to complex S increased, the more complex W were formed gradually, however, the more non-specific SDA products also be obtained. In order to ensure a high-efficiency and specific reaction and reduce the background signal, the ratio of strand F to complex S was selected as 1.5:1 for further experiment.

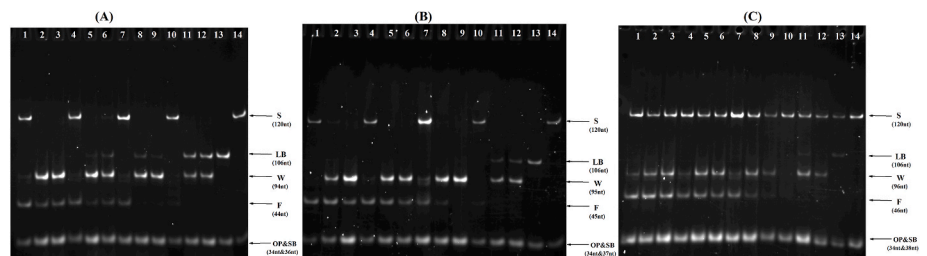


Fig. 3. Polyacrylamide gel electropherograms of different reaction systems: the toehold region $\bar{5}$ and toehold region $\bar{3}$ were (A) 6 nt/4 nt, (B) 5 nt/5 nt, and (C) 4 nt/6 nt; the concentration ratios of F strand to substrate probe were 0.5:1 (lanes 10–12), 1:1 (lanes 7–9), 1.5:1 (lane 4–6), and 2:1 (lane 1–3); lanes 1, 4, 7, and 10 were control groups, lane 13 was C, lane 14 was S. Abbreviation: three-stranded substrate complex (S), catalyst strand (C), fuel strand (F) output strand (OB), signal strand (SB), linker strand (LB), and waste complex (W).

3.5. Optimization of MB strand

The molecular beacon strand is composed of a short arm with only a few base pairs and a long loop region. The short arm is conducive to rapid conversion of signals, and also affects the stability of the MB strand. In this study, two MB strands (the sequences were shown in Table S1), with different-stability short arm, were designed by NUPACK software, and the fluorescence signal conversion performance of these MB strands was investigated. It was found that MB1 strand with lower-stability arm show higher PL intensity than MB2 strand (Fig. 4). For this reason, MB1 strand was applied to signal conversion and modified on the surface of g-CNQDs@Zn-MOF.

3.6. Sensitivity and linearity of the biosensor

Next, the linear range and sensitivity of the fluorescence biosensor were evaluated. A series of concentrations of N protein was determined using this biosensor. As shown in Fig. 5A, the fluorescence signal of the proposed biosensor varied with the concentration of N protein, and the results confirmed that the fluorescence intensity was in good linearity with the concentration of N protein in the range of 5.0 pg/mL~ 1.0×10^3 pg/mL. The correction equation is $y = 2.626x + 191.4$ ($R^2 = 0.9984$), the detection limit (DL) and the quantification limit (QL) were 1.0 pg/mL ($S/N = 3$) and 3.4 pg/mL ($S/N = 10$), respectively. The control experiments only using conformational entropy DNA circuit was carried out in pre-experiment, the detection limit was 50 pg/mL, which showed that the sensitivity of the sensor was increased by nearly 50-fold using g-CNQDs@Zn-MOF as a signal enhancement strategy than that of no nanomaterials. Compared with the reported biosensors (Table S2), the established biosensor based on conformational entropy-driven DNA circuit has a lower detection limit and a wider linear range, which can meet the requirements of rapid detection of SARS-CoV-2 in food samples.

3.7. Specificity and stability of the sensor

Besides, N protein of SARS-CoV-2 was analyzed with the fluorescence biosensor, N proteins of HCoV-OC43, HCoV-HKU1, MERS-CoV, and SARS-CoV were also measured to evaluate the specificity of this biosensor. The results were demonstrated in Fig. 5B, obvious fluorescent signal for the target analyte was obtained, while no significant responses for the non-targets were observed. The N-48 aptamer was specific to the N protein of SARS-CoV-2, thus specifically triggered conformational entropy-driven circuit, which leads to an increase of the fluorescent signal in the analysis system. While other analyte can't be recognized by N-48 aptamer, thus no obvious fluorescent signal, basically the same as the background signal, was obtained. The results confirmed that the fluorescence biosensor has good selectivity for the N protein of SARS-CoV-2, and can effectively distinguish the analyte and interfering components.

To evaluate the stability of the biosensor, the reaction system, including the complex S, strand C, strand F, N-48 and MB strand, was prepared and stored at 4 °C. The SARS-CoV-2 N proteins solutions, with the concentration of 100 pg/mL, were determined with the biosensing

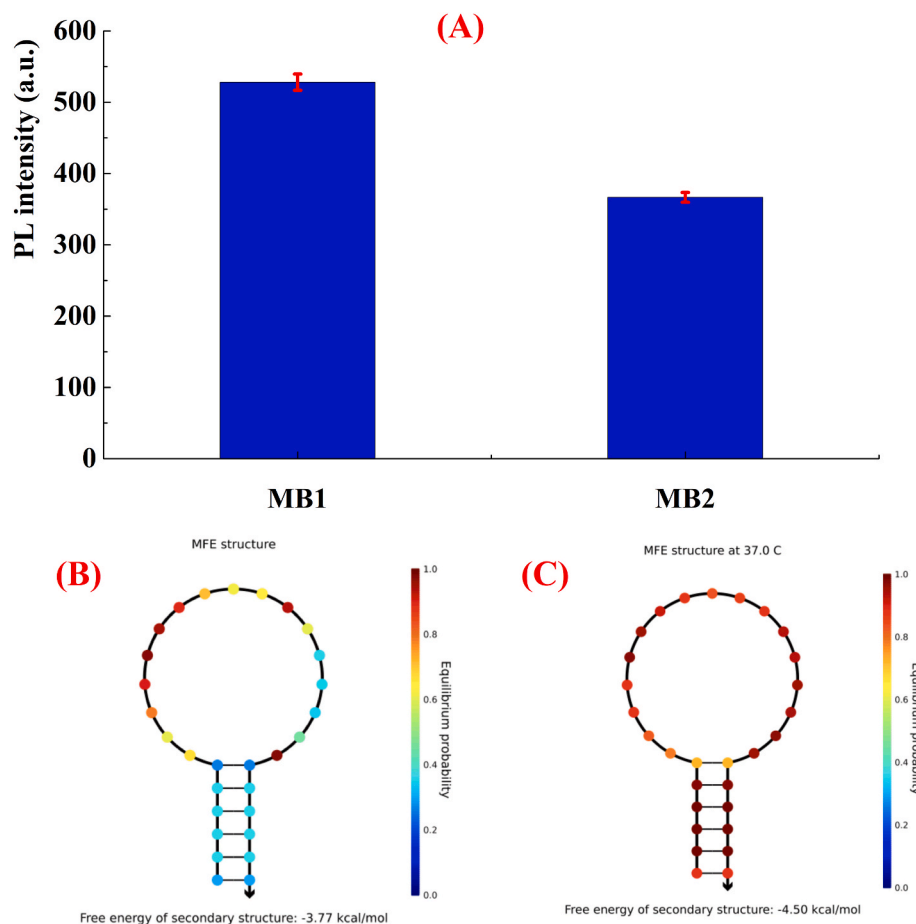


Fig. 4. (A) The PL intensities of conformational entropy-driven circuit system with MB1 strand or MB2 strand; Structures of (B) MB1 strand and (C) MB2 strand. The error bars represent the standard deviations of three independent experiment. Abbreviation: molecular beacon (MB).

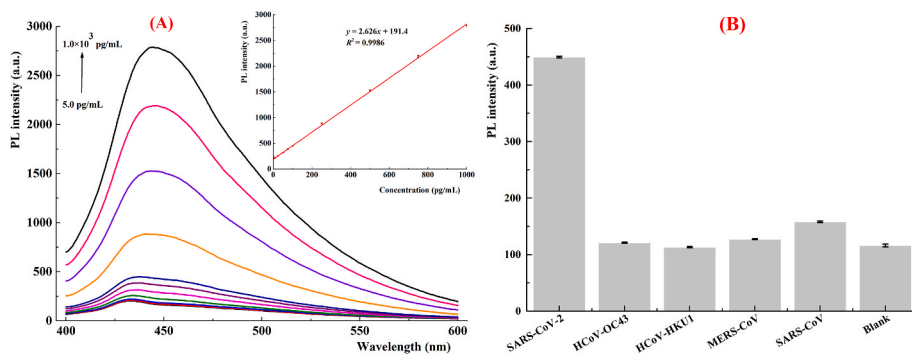


Fig. 5. (A) Fluorescence emission spectra overlay for detection of SARS-CoV-2 N protein in the linear range of 5.0 pg/mL~ 1.0×10^3 pg/mL; the calibration plot for the concentration of N protein and PL intensity acquired by the fluorescence biosensor; (B) Selectivity evaluation of the proposed biosensor for the detection of N protein of SARS-CoV-2 against other four kinds of proteins (the concentration of all proteins used in the experiment was 100 pg/mL). The error bars represent the standard deviations of three independent experiment.

strategy every 3 days for 15 days, and the PL intensity was 451.0 a.u., 450.2 a.u., 453.3 a.u., 449.6 a.u., 447.3 a.u., 451.7 a.u., respectively, which demonstrated that the fluorescence biosensor had good stability.

In order to assess the reproducibility of the sensing strategy, six fluorescence biosensors based on conformational entropy-driven DNA circuit were prepared, and were applied to the analysis of one actual frozen shrimp sample (positive sample) under the same conditions. The results showed that the RSD of the 6 results was 2.62%, and this sensor had good reproducibility due to simple preparation process, simple operation and enzyme-free reaction.

3.8. Determination of actual samples

For the purpose of applicability evaluation, 64 cold-chain food products (including cherry, frozen shrimp, salmon, and frozen fish) were sampled with swab method. After heating at 95 °C for 10 min (Fig. S4), the N proteins of SARS-Cov-2 were released and sample solution was analyzed with the fluorescence aptasensor and RT-PCR, respectively (Fig. S5). According to fluorescence aptasensor correctly identified 30/30 samples as positive and 34/34 samples as negative, exhibiting 100% sensitivity, specificity, positive predictive value, negative predictive value, and concordance with RT-PCR (Table S3). In all cases, the PL intensity correlated well with the Ct-value (Table S4). Therefore, the fluorescence biosensor based on conformational entropy-driven DNA

circuit has excellent performance in preliminary practical applications, which meet the determination requirements of actual samples. Consequently, this sensing strategy could be employed for rapid detection of SARS-CoV-2 in food samples. Finally, an important work in the future is to implement higher-order DNA assemblies such as a three-way or four-way junction for multiple conformational entropy-driven DNA circuit. Thereby obtaining high-throughput and multi-channel signal gain.

4. Conclusion

To sum up, we have successfully established a robust fluorescence biosensor based on nonenzymatic DNA circuit and demonstrated the potential of conformational entropy-driven circuit as powerful signal amplification. In this assay, each reaction starts from substrate complex (S): conformational entropy-driven circuit releases amounts of SB, while the hybridization of MB strands and SB unfolded hairpin structure of MB and separated the fluorescence donors with quenching groups, thereby releasing a fluorescence signal. Moreover, the introduction of N-48 aptamer provided a direct molecular bridge between N protein and DNA, enabling sensitive and highly specific sensing of SARS-CoV-2. The main achievement was that DNA circuits could be readily matched and mixed due to the supernormal programmability provided by conformational entropy and interactions of base-pairing. Compared with the previous SDA based on the hairpin substrates, the signal leakage of the linear DNA-based SDA driven by conformational entropy is much lower, and this conformational entropy-driven circuit could amplify signals significantly while keeping lower background by rational sequence design. Comparable to no amplification, the conformational entropy-driven circuit combined with g-CNQDs@Zn-MOF could amplify 50-fold signal, without sacrificing its specificity within 30 min. Besides, the stability and reproducibility of this fluorescence biosensor are significantly enhanced. Moreover, as a variety of aptamers are either available or can be obtained through SELEX for a broad range of targets, the conformational entropy-driven DNA circuits developed in this study could be used for other targets analysis. Finally, an important work in the future is to implement higher-order DNA assemblies such as a three-way or four-way junction for multiple conformational entropy-driven circuit, thereby obtaining high-throughput and multi-channel signal gain.

CRedit authorship contribution statement

Chen Zhou: Resources, Conceptualization, Methodology, Investigation, Formal analysis, Writing – original draft. **Chiliang Lin:** Methodology, Investigation. **Yuyao Hu:** Methodology, Investigation. **Haocheng Zan:** Methodology, Investigation. **Xiaruiyan Xu:** Methodology, Investigation. **Chengjun Sun:** Investigation, Formal analysis. **Haimin Zou:** Methodology, Investigation, Formal analysis, Writing – original draft. **Yongxin Li:** Supervision, Writing – original draft.

Declaration of competing interest statement

The authors declare that they have no known competing financial interests or personal relationships that could have appeared to influence the work reported in this paper.

Data availability

Data will be made available on request.

Acknowledgements

We acknowledge the support funded by China Postdoctoral Science Foundation (Grant No.: 2019M663531, and BX20190221), Chengdu Municipal Bureau on Science and Technology (Grant No.: 2021-YF05-00592-SN), and Key Research and Development Program of Sichuan

Province (Grant No.: 2021YFS0005).

Appendix A. Supplementary data

Supplementary data to this article can be found online at <https://doi.org/10.1016/j.lwt.2022.114032>.

References

- Bocková, M., Slabý, J., Špringer, T., & Homola, J. (2019). Advances in surface plasmon resonance imaging and microscopy and their biological applications. *Annual Review of Analytical Chemistry*, 12(1), 151–176. <https://doi.org/10.1146/annurev-anchem-061318-115106>
- Ceylan, Z., Meral, R., & Cetinkaya, T. (2020). Relevance of SARS-CoV-2 in food safety and food hygiene: Potential preventive measures, suggestions and nanotechnological approaches. *Virusdisease*, 31(2), 154–160. <https://doi.org/10.1007/s13337-020-00611-0>
- Chen, Z., Wu, Q., Chen, J., Ni, X., & Dai, J. (2020). A DNA aptamer based method for detection of SARS-CoV-2 nucleocapsid protein. *Virologica Sinica*, 35(3), 351–354. <https://doi.org/10.1007/s12250-020-00236-z>
- Chi, Y., Wang, Q., Chen, G., & Zheng, S. (2021). The long-term presence of SARS-CoV-2 on cold-chain food packaging surfaces indicates a new COVID-19 winter outbreak: A mini review. *Frontiers in Public Health*, 9, Article 650493. <https://doi.org/10.3389/fpubh.2021.650493>
- De la Paz, E., Barfidokht, A., Rios, S., Brown, C., Chao, E., & Wang, J. (2021). Extended noninvasive glucose monitoring in the interstitial fluid using an epidermal biosensing patch. *Analytical Chemistry*. <https://doi.org/10.1021/acs.analchem.1c02887>
- Fan, Z., Yao, B., Ding, Y., Zhao, J., Xie, M., & Zhang, K. (2021). Entropy-driven amplified electrochemiluminescence biosensor for RdRp gene of SARS-CoV-2 detection with self-assembled DNA tetrahedron scaffolds. *Biosensors and Bioelectronics*, 178, Article 113015. <https://doi.org/10.1016/j.bios.2021.113015>
- Fu, Y., Yu, Q., Zhang, Q., Zhang, X., Du, C., & Chen, J. (2021). A photocurrent-polarity-switching biosensor for highly selective assay of mucin 1 based on target-induced hemin transfer from ZrO(2) hollow spheres to G-quadruplex nanowires. *Biosensors and Bioelectronics*, 192, Article 113547. <https://doi.org/10.1016/j.bios.2021.113547>
- Godoy, M. G., Kibenge, M. J. T., & Kibenge, F. S. B. (2021). SARS-CoV-2 transmission via aquatic food animal species or their products: A review. *Aquaculture*, 536, Article 736460. <https://doi.org/10.1016/j.aquaculture.2021.736460>
- Haddow, A. D., Watt, T. R., Bloomfield, H. A., Shamblyn, J. D., Dyer, D. N., & Harbourt, D. E. (2020). Stability of SARS-CoV-2 on produce following a low-dose aerosol exposure. *The American Journal of Tropical Medicine and Hygiene*, 103(5), 2024–2025. <https://doi.org/10.4269/ajtmh.20-1033>
- Huilai, M., Zhaoqun, W., Xiang, Z., Jun, H., Yong, Z., Hong, W., ... Wenbo, X. (2021). Outbreak reports: Long distance transmission of SARS-CoV-2 from contaminated cold chain products to humans — Qingdao city, Shandong Province, China, September 2020. *China CDC Weekly*, 2(30), 637–644. <https://doi.org/10.46234/ccdcw2021.164>
- Kirtipal, N., Bharadwaj, S., & Kang, S. G. (2020). From SARS to SARS-CoV-2, insights on structure, pathogenicity and immunity aspects of pandemic human coronaviruses. *Infection, Genetics and Evolution*, 85, Article 104502. <https://doi.org/10.1016/j.meegid.2020.104502>
- Kong, Y., Cheng, Q., He, Y., Ge, Y., Zhou, J., & Song, G. (2020). A dual-modal fluorometric and colorimetric nanoprobe based on graphitic carbon nitride quantum dots and Fe(II)-bathophenanthroline complex for detection of nitrite in sausage and water. *Food Chemistry*, 312, Article 126089. <https://doi.org/10.1016/j.foodchem.2019.126089>
- Kumagai, K., Uematsu, T., Torimoto, T., & Kuwabata, S. (2019). Direct surface modification of semiconductor quantum dots with metal-organic frameworks. *CrystEngComm*, 21(37), 5568–5577. <https://doi.org/10.1039/c9ce00769e>
- Leung, K. K., Downs, A. M., Ortega, G., Kurnik, M., & Plaxco, K. W. (2021). Elucidating the mechanisms underlying the signal drift of electrochemical aptamer-based sensors in whole blood. *ACS Sensors*. <https://doi.org/10.1021/acscensors.1c01183>
- Liu, P., Yang, M., Zhao, X., Guo, Y., Wang, L., Zhang, J., ... Wu, G. (2020). Cold-chain transportation in the frozen food industry may have caused a recurrence of COVID-19 cases in destination: Successful isolation of SARS-CoV-2 virus from the imported frozen cod package surface. *Biosaf Health*, 2(4), 199–201. <https://doi.org/10.1016/j.bshealth.2020.11.003>
- Liu, M., Zhang, Q., Kannan, B., Botton, G. A., Yang, J., Soleymani, L., ... Li, Y. (2018). Self-Assembled functional DNA superstructures as high-density and versatile recognition elements for printed paper sensors. *Angewandte Chemie International Edition in English*, 57(38), 12440–12443. <https://doi.org/10.1002/anie.201806489>
- Louidice, A., Saris, S., Oveisi, E., Alexander, D. T. L., & Buonsanti, R. (2017). CsPbBr(3) QD/AlO(x) inorganic nanocomposites with exceptional stability in water, light, and heat. *Angewandte Chemie International Edition in English*, 56(36), 10696–10701. <https://doi.org/10.1002/anie.201703703>
- Lopreside, A., Montali, L., Wang, B., Tassoni, A., Ferri, M., Calabretta, M. M., et al. (2021). Orthogonal paper biosensor for mercury(II) combining bioluminescence and colorimetric smartphone detection. *Biosensors and Bioelectronics*, 194, Article 113569. <https://doi.org/10.1016/j.bios.2021.113569>
- Owen, J., & Brus, L. (2017). Chemical synthesis and luminescence applications of colloidal semiconductor quantum dots. *Journal of the American Chemical Society*, 139(32), 10939–10943. <https://doi.org/10.1021/jacs.7b05267>

- Ozma, M. A., Maroufi, P., Khodadadi, E., Köse, Ş., Esposito, I., Ganbarov, K., ... Kafil, H. S. (2020). Clinical manifestation, diagnosis, prevention and control of SARS-CoV-2 (COVID-19) during the outbreak period. *Infezioni in Medicina, Le*, 28(2), 153–165.
- Pan, Y., Wei, X., Guo, X., Wang, H., Song, H., Pan, C., et al. (2021). Immunoassay based on Au-Ag bimetallic nanoclusters for colorimetric/fluorescent double biosensing of dicofol. *Biosensors and Bioelectronics*, 194, Article 113611. <https://doi.org/10.1016/j.bios.2021.113611>
- Ragavan, K. V., Kumar, S., Swaraj, S., & Neethirajan, S. (2018). Advances in biosensors and optical assays for diagnosis and detection of malaria. *Biosensors and Bioelectronics*, 105, 188–210. <https://doi.org/10.1016/j.bios.2018.01.037>
- Rahimi, A., Mirzazadeh, A., & Tavakolpour, S. (2021). Genetics and genomics of SARS-CoV-2: A review of the literature with the special focus on genetic diversity and SARS-CoV-2 genome detection. *Genomics*, 113(1 Pt 2), 1221–1232. <https://doi.org/10.1016/j.ygeno.2020.09.059>
- Reiss, P., Protière, M., & Li, L. (2009). Core/Shell semiconductor nanocrystals. *Small*, 5(2), 154–168. <https://doi.org/10.1002/sml.200800841>
- Selby, L. I., Aurelio, L., Yuen, D., Graham, B., & Johnston, A. P. R. (2018). Quantifying cellular internalization with a fluorescent click sensor. *ACS Sensors*, 3(6), 1182–1189. <https://doi.org/10.1021/acssensors.8b00219>
- Shao, F., Mi, L., Tian, Z., Zheng, C., Zhang, Y., Li, Q., et al. (2019). Promoting photodegradation efficiency via a heterojunction photocatalyst combining with oxygen direct and fast diffusion from the gas phase to active catalytic sites. *ACS Applied Materials & Interfaces*, 11(47), 44922–44930. <https://doi.org/10.1021/acsaami.9b17122>
- Sun, Z., Sun, Y., Yang, M., Jin, H., & Gui, R. (2021). A petal-shaped MOF assembled with a gold nanocage and urate oxidase used as an artificial enzyme nanohybrid for tandem catalysis and dual-channel biosensing. *Nanoscale*, 13(30), 13014–13023. <https://doi.org/10.1039/d1nr02688g>
- Sun, H., Yang, Z., Wei, M., Sun, W., Li, X., Ye, S., ... Seferos, D. S. (2017). Chemically addressable perovskite nanocrystals for light-emitting applications. *Advanced Materials*, 29(34). <https://doi.org/10.1002/adma.201701153>
- Vashisht, D., Sharma, E., Kaur, M., Vashisht, A., Mehta, S. K., & Singh, K. (2020). Solvothermal assisted phosphate functionalized graphitic carbon nitride quantum dots for optical sensing of Fe ions and its thermodynamic aspects. *Spectrochimica Acta Part A: Molecular and Biomolecular Spectroscopy*, 228, Article 117773. <https://doi.org/10.1016/j.saa.2019.117773>
- Vermisoglou, E., Panáček, D., Jayaramulu, K., Pykal, M., Frébort, I., Kolář, M., ... Otyepka, M. (2020). Human virus detection with graphene-based materials. *Biosensors and Bioelectronics*, 166, Article 112436. <https://doi.org/10.1016/j.bios.2020.112436>
- Wang, W., Gong, Z., Yang, S., Xiong, T., Wang, D., & Fan, M. (2020). Fluorescent and visual detection of norfloxacin in aqueous solutions with a molecularly imprinted polymer coated paper sensor. *Talanta*, 208, Article 120435. <https://doi.org/10.1016/j.talanta.2019.120435>
- Wang, M. Y., Zhao, R., Gao, L. J., Gao, X. F., Wang, D. P., & Cao, J. M. (2020). SARS-CoV-2: Structure, biology, and structure-based therapeutics development. *Frontiers in Cellular and Infection Microbiology*, 10, Article 587269. <https://doi.org/10.3389/fcimb.2020.587269>
- Yang, G., Xiao, Z., Tang, C., Deng, Y., Huang, H., & He, Z. (2019). Recent advances in biosensor for detection of lung cancer biomarkers. *Biosensors and Bioelectronics*, 141, Article 111416. <https://doi.org/10.1016/j.bios.2019.111416>
- Yekta, R., Vahid-Dastjerdi, L., Norouzbeigi, S., & Mortazavian, A. M. (2021). Food products as potential carriers of SARS-CoV-2. *Food Control*, 123, Article 107754. <https://doi.org/10.1016/j.foodcont.2020.107754>
- Yousefi, H., Ali, M. M., Su, H. M., Filipe, C. D. M., & Didar, T. F. (2018). Sentinel wraps: Real-time monitoring of food contamination by printing DNzyme probes on food packaging. *ACS Nano*, 12(4), 3287–3294. <https://doi.org/10.1021/acsnano.7b08010>
- Zhang, L., Fang, X., Liu, X., Ou, H., Zhang, H., Wang, J., ... Luo, Z. (2020). Discovery of sandwich type COVID-19 nucleocapsid protein DNA aptamers. *Chem Commun (Camb)*, 56(70), 10235–10238. <https://doi.org/10.1039/d0cc03993d>
- Zhang, D. Y., Turberfield, A. J., Yurke, B., & Winfree, E. (2007). Engineering entropy-driven reactions and networks catalyzed by DNA. *Science*, 318(5853), 1121–1125. <https://doi.org/10.1126/science.1148532>
- Zhao, Y., Tong, R. J., Xia, F., & Peng, Y. (2019). Current status of optical fiber biosensor based on surface plasmon resonance. *Biosensors and Bioelectronics*, 142, Article 111505. <https://doi.org/10.1016/j.bios.2019.111505>
- Zhou, C., Zou, H., Sun, C., Ren, D., Chen, J., & Li, Y. (2018). Signal amplification strategies for DNA-based surface plasmon resonance biosensors. *Biosensors and Bioelectronics*, 117, 678–689. <https://doi.org/10.1016/j.bios.2018.06.062>